Neutron Reflection Studies on Segment Distribution of Block Chains in Lamellar Microphase-Separated Structures

Naoya Torikai and Ichiro Noda

Department of Applied Chemistry, Graduate School of Engineering, Nagoya University, Furo-cho, Chikusa-ku, Nagoya 464-01, Japan

Alamgir Karim, Sushil K. Satija, and Charles C. Han

National Institute of Standards and Technology, Gaithersburg, Maryland 20899

Yushu Matsushita*

Neutron Scattering Laboratory, The Institute for Solid State Physics, The University of Tokyo, Tokai, Naka-gun, Ibaraki 319-11, Japan

Toshihiro Kawakatsu

Department of Physics, Tokyo Metropolitan University, Minami-ohsawa 1-1, Hachioji-shi, Tokyo 192-03, Japan

Received July 23, 1996; Revised Manuscript Received March 10, 1997[⊗]

ABSTRACT: Segment distribution of styrene in an alternating lamellar structure of styrene−2-vinylpyridine diblock copolymer was investigated by neutron reflection. Block copolymers having three types of deuterium-labeled styrene block chains consisting of fully labeled, partially junction-labeled, and partially end-labeled block chains were used in this study. The degree of junction and end labeling was varied to obtain a more complete picture of segment distribution. Spin-coated thin films of these block copolymers on silicon wafers exhibited lamellar structures which were oriented preferentially parallel to the silicon surface. Our results indicate that the poly(2-vinylpyridine) block chain exists at the silicon surface, while polystyrene appears at the air surface in all of the film specimens. The segment distribution at the interface between polystyrene and poly(2-vinylpyridine) lamellae could be well described by an error function. The thickness of the lamellar interface (defined as a full-width half-maximum value of the error function) is evaluated to be about 4.5 nm, suggesting that the blocks are strongly segregated. Accordingly, the segments of a block chain in the vicinity of the chemical junction point between two block chains are determined to be strongly localized near the lamellar interface. However, the free ends are broadly distributed throughout the lamellar microdomain with their net maximum distribution at the center of each microdomain. Such an end-segment distribution of the block chains is shown to be consistent with predictions from a mean field theory.

Introduction

Diblock copolymers with two incompatible block chains are known to form a variety of microphase-separated structures such as spheres, cylinders, lamellae, etc., depending upon their compositions.[1,2] The alternating lamellar structure has been studied most intensively so far, because of its simple geometry in addition to the ease by which its "equilibrium" state is achievable in comparison to other structures.[3] Most previous studies have determined that the lamellar domain spacing is proportional to about the $^2/_3$ power of the molecular weight of the diblock copolymer.[4,5] Small-angle neutron scattering (SANS) measurements have revealed that the block chains in the lamellar microdomain are extended along the direction perpendicular to the lamellar interface but are shrunk along the direction parallel to the interface so as to keep the volumes occupied by their segments unchanged.[6,7] This is an area of some controversy since theories on microphase separation in the strong segregation limit[8−12] can readily predict the extension of block chains along the direction perpendicular to the lamellar interface, but not the shrinkage along the parallel direction. Thus a study of the localization of block segments near and away from the junction point is important to resolve such issues.

In our previous SANS studies on styrene−2-vinylpyridine diblock copolymers (PS−P2VP) with partially deuterium-labeled PS block chains,[13] the location of labeled sections of block chain within the lamellar microdomain as well as their conformations was investigated. It was observed that the part of a block chain near the chemical junction point between the two block chains is localized close to the lamellar interface, and additionally is shrunk along the direction parallel to the lamellar interface to the same extent as a whole block chain of the same molecular weight. On the other hand, the labeled part at the free end is localized at the center of the lamellar microdomain and its dimension parallel to the lamellar interface is almost the same as that of the unperturbed chain of the same molecular weight. However, information on the degree of localization of these parts of a block chain could not be obtained in our previous work, since SANS is not sensitive enough to yield detailed distributions of the deuterium-labeled parts. Recently, Russell and co-workers[14,15] minutely investigated the segment distributions of block chains in a lamellar structure of styrene−methyl methacrylate diblock copolymer (PS−PMMA), which has a Flory−Huggins interaction parameter χ (=0.041 at 298 K[16]) much lower than that of PS−P2VP (χ = 0.088 at 298 K[17]). They used neutron reflectivity (NR), which is a powerful technique for the study of surfaces and interfaces owing to its high spatial resolution. For PS−PMMA, Russell et al. observed that the segments of

[⊗] Abstract published in *Advance ACS Abstracts,* May 1, 1997.

S0024-9297(96)01089-3 CCC: $14.00

Table 1. Molecular Characteristics of Deuterium-Labeled Styrene−2-Vinylpyridine Block Copolymers

sample code[a]	$10^{-3}M_n$[b]	M_w/M_n	Φ[d]
DP-77	(**92**)−75	1.09	(**0.50**)−0.50
SDP-5	(30−**17**)−42	1.02	(0.33−**0.18**)−0.49
SDP-6	(45−**4**)−46	1.14	(0.55−**0.03**)−0.42
DSP-2	(**17**−37)−45	1.03	(**0.18**−0.39)−0.43
DSP-3	(**7**[c]−41)−51	1.02	(**0.07**−0.47)−0.46

[a] The letters D, S, and P denote styrene-d_8, styrene-h_8, and 2-vinylpyridine block chains, respectively. [b] The boldfaced figure denotes the molecular weight of the styrene-d_8 (D) block chain. [c] This molecular weight was calculated from the molecular weight of the total styrene (D + S) block chain and the weight fraction of D in the total styrene block chain. [d] Φ is the volume fraction of each block chain determined by a combination of elemental analysis and pyrolysis−gas chromatography. The boldfaced figure denotes that of the D block chain.

block chain adjacent to the chemical junction point are strongly localized at the lamellar interface, while those at the free end are widely distributed within the lamellar microdomain, with a weak maximum in their overall distribution at the center of the lamella.[14] An effective width of the lamellar interface in PS−PMMA was evaluated to be about 5 nm, regardless of the molecular weight of the diblock copolymer.[15] This width is much larger than that evaluated for the styrene−isoprene diblock copolymer (2 nm), which has a much higher χ value (χ = 0.14 at 298 K) than that of PS−PMMA, determined by small-angle X-ray scattering (SAXS).[5] Such trends provide additional motivating factors to study the segment distributions of block chains in the lamellar microdomain of a well-defined diblock copolymer with a χ value different from that of PS−PMMA, using the NR technique.

For this work we prepared PS−P2VPs having fully and partially deuterium-labeled styrene block chains and investigated the distributions of these labeled segments in the lamellar microdomain by NR. Two pairs of partially center- and end-labeled block copolymers with almost the same overall molecular weights but with different contents of the labeled segments were prepared to compare directly the distributions of the chain ends with those adjacent to the junctions. These distributions are further compared with those of PS−PMMA, reported by Russell et al.,[14,15] to establish a systematic trend of the effects of χ parameter magnitude on segment distributions of the block chain in a lamellar microdomain.

Experimental Section

Samples used for this study comprised a styrene-d_8−2-vinylpyridine (DP) diblock copolymer and two center-labeled and two end-labeled triblock copolymers: poly(styrene-h_8-*b*-styrene-d_8-*b*-2-vinylpyridine) (SDP) and poly(styrene-d_8-*b*-styrene-h_8-*b*-2-vinylpyridine) (DSP). All samples were prepared by anionic polymerization with the sequential monomer addition technique. The preparation methods for the samples have been reported previously.[18] Important molecular characteristics of the samples used are listed in Table 1. The content of the deuterium-labeled section, styrene-d_8, in the styrene block chain was determined using pyrolysis−gas chromatography.[19] As preliminary information, SAXS studies on "thick" film specimens, 0.1−0.2 mm thick, prepared by solvent-casting indicated that all samples exhibit lamellar structures.[6,13]

One-side polished silicon wafers, 10 cm in diameter and 5 mm in thickness, were purchased from Semiconductor Processing Co.[20] The silicon wafers were immersed into a strong oxidizing bath containing concentrated sulfuric acid and 30% hydrogen peroxide in the volume ratio of 7:3, to remove any organic impurities. They were then thoroughly rinsed using deionized water, dried by blowing helium gas, and immediately spin-coated. Thin film specimens for reflectivity measurements were prepared by spin-coating from toluene solutions containing about 2% block copolymers by weight on the silicon wafers at 2 × 10^3 rpm, and then annealed under vacuum at 150 °C for 3 days. The thicknesses of all films thus prepared were determined to be between 120 and 250 nm by X-ray reflectivity measurements.

Table 2. Coherent Scattering Length Densities, *b*/*v*, of Materials

material	$10^4 b/v$ (nm^{-2})	material	$10^4 b/v$ (nm^{-2})
air	0	poly(2-vinylpyridine)	1.95
poly(styrene-h_8)	1.41	SiO_2	3.48
poly(styrene-d_8)	6.47	Si	2.09

Neutron reflectivity measurements were performed on two reflectometers, BT-7 and NG-7, at the National Institute of Standards and Technology, Gaithersburg, MD. The wavelength, λ, of the neutron beam used was 0.237 nm with a wavelength spread, $\Delta\lambda/\lambda$, of 1.7% for the BT-7 reflectometer, and 0.41 nm with a spread of 4% for the NG-7 reflectometer. The essential difference between the two reflectometers lies in their geometries: film specimens are set vertically on BT-7, while the reflecting plane was horizontal on NG-7. However, the use of two reflectometers was for purposes of convenience of measurement scheduling and does not reflect any advantage for this study. The reflectivity of DP-77 was measured on NG-7, and all others were on BT-7. In this study we observed specular reflection, where the incident angle of the neutron beam irradiated on the film surface, θ_{in}, is equal to the reflected angle, θ_{out}, as a function of neutron momentum transfer in air, q [=$(4\pi/\lambda)\sin\theta$], perpendicular to the film surface.

Reflectivities were calculated from model scattering length density (b/v) profiles along the direction perpendicular to the film surface by using an algorithm of Parratt based on a recursive calculation method,[21,22] and fitted to the measured reflectivities. This algorithm is suitable for calculating the reflectivity of a multilayer system with distinct interfaces between each layer, whose b/v profile is represented by a series of step functions. However, the actual air/film and film/silicon interfaces and between microdomains must have finite thicknesses. Furthermore, the distributions of labeled parts of a block chain in the microdomains must be smooth rather than distinct. In all these places, the b/v profiles must change smoothly. Therefore, such regions were approximately regarded as an assembly of several distinct layers with b/v profiles represented by step functions. Further discretization of step height did not affect the calculated reflectivity visually. Fittings of the calculated reflectivities to the measured data were performed by assuming that the microphase-separated structures formed in the thin films are nearly in equilibrium, so that a single structural unit is repeated periodically inside the films. The b/v values for pure materials required for calculation of reflectivity are listed in Table 2.

Results

In this section we present our analysis of NR data, to be discussed and interpreted later in the Discussion. Figure 1a shows a reflectivity profile of a diblock copolymer, DP-77, having a fully deuterium-labeled styrene block chain, as a function of q. The experimental profile, represented by the open circles, shows Bragg peaks up to several orders in the high-q region, indicating the existence of a highly-ordered structure perpendicular to the film surface. The solid line in the figure is the best-fitted reflectivity profile calculated from a b/v profile normal to the film surface shown in Figure 1b.[23] A close comparison between the two reflectivity profiles in Figure 1a shows that the calculated Bragg

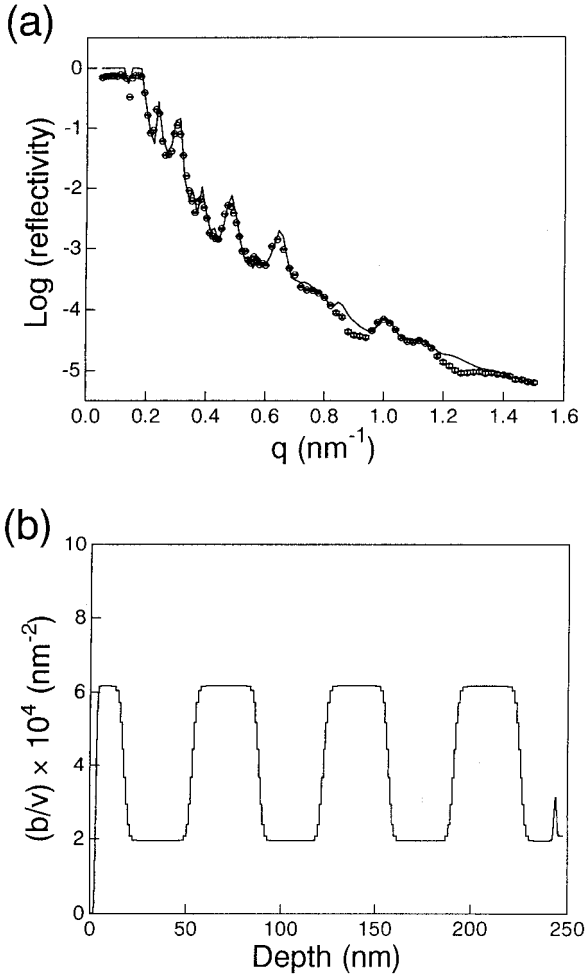

Figure 1. (a) Neutron reflectivity from a diblock copolymer, DP-77, as a function of neutron momentum transfer, q, perpendicular to the film surface. Open circles denote experimental data, while the solid line indicates the best-fitted curve calculated from the scattering length density profile shown in (b). (b) Coherent scattering length density profile along the direction perpendicular to the film surface.

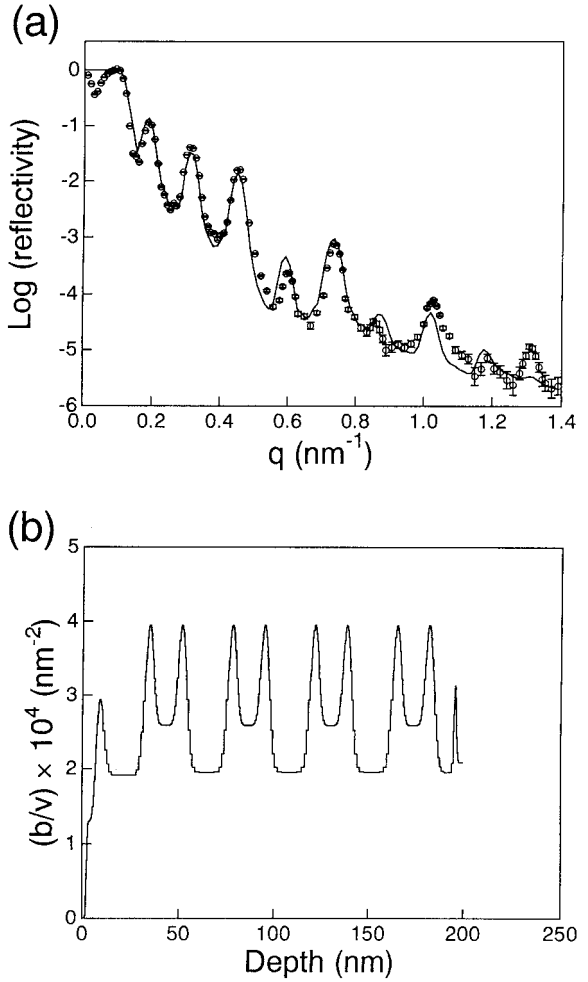

Figure 2. (a) Reflectivity profile of a center-labeled block copolymer, SDP-5, of which the styrene-d_8 (D) content within the polystyrene block chain is 35 vol %. (b) Its scattering length density profile.

peak intensities are slightly higher than the experimental ones. If the Bragg peak intensities were fitted by changing the b/v contrast between lamellae, the calculated reflectivity profile deviates from the experimental one in the high-q region. Since the thickness of the lamellar interface reflects mainly on the q dependence of reflectivity in the high-q region, we gave priority to the agreement of reflectivity profiles in the high-q region in the actual fitting procedure. Moreover, the reduction of reflectivity in the total reflection region can be attributed to the finite sample size at low q, which was not taken into account in the calculations. However, this does not affect our data analysis over the q range where finite sample size effects are absent. The b/v profile reveals that the poly(styrene-d_8) lamellae with a higher b/v value of 6.2×10^{-4} nm^{-2} and poly(2-vinylpyridine) (P2VP) lamellae with a lower b/v value of 1.9×10^{-4} nm^{-2} are stacked alternately throughout the film with a preferential orientation parallel to the silicon surface. From this figure the lamellar domain spacing, L_{NR}, is evaluated to be 69 nm. A polystyrene lamella whose thickness is one-half of the corresponding normal lamella is formed on top of the thin film because of its lower surface energy compared to that of P2VP. On the other hand, a P2VP lamella whose thickness is one-half of the normal lamella is formed at the bottom of the film because of its higher affinity for the SiO_2 layer covering the silicon surface, which can be recognized as a sharp peak, about 1.5 nm thick, on the right side of Figure 1b. The segment distribution at the interface between polystyrene and P2VP lamellae can be well described by an error function, and the interfacial thickness, defined as the full-width at half-maximum value of the interfacial profile, is evaluated to be about 4.5 nm. If the hyperbolic tangent function which described well the interfacial profile between PS−PMMA lamellae[15] was used instead of the error function, the quality of fit to the experimental data degraded noticeably.

The reflectivity profiles from two center-labeled block copolymers with different amounts of styrene-d_8 (D) segments, SDP-5 and -6, are shown in Figures 2a and 3a, respectively. Both profiles have distinct Bragg peaks that extend well into the hig-q region, indicating a strong ordering of the D segments perpendicular to the film surface. The best-fitted b/v profiles for SDP-5 and -6 are shown in Figures 2b and 3b, respectively. In both cases the b/v profiles corresponding to the polystyrene lamellae have sharp twin peaks near the lamellar interface toward the P2VP lamellae with $b/v = 1.9 \times 10^{-4}$ nm^{-2}. All the peaks in these b/v profiles are produced by changing the combination of error functions to fit the calculated reflectivity profiles with the experimental data. L_{NR}'s evaluated from these b/v profiles are about 43 nm, and the widths of the lamellar interface of both center-labeled block copolymers were

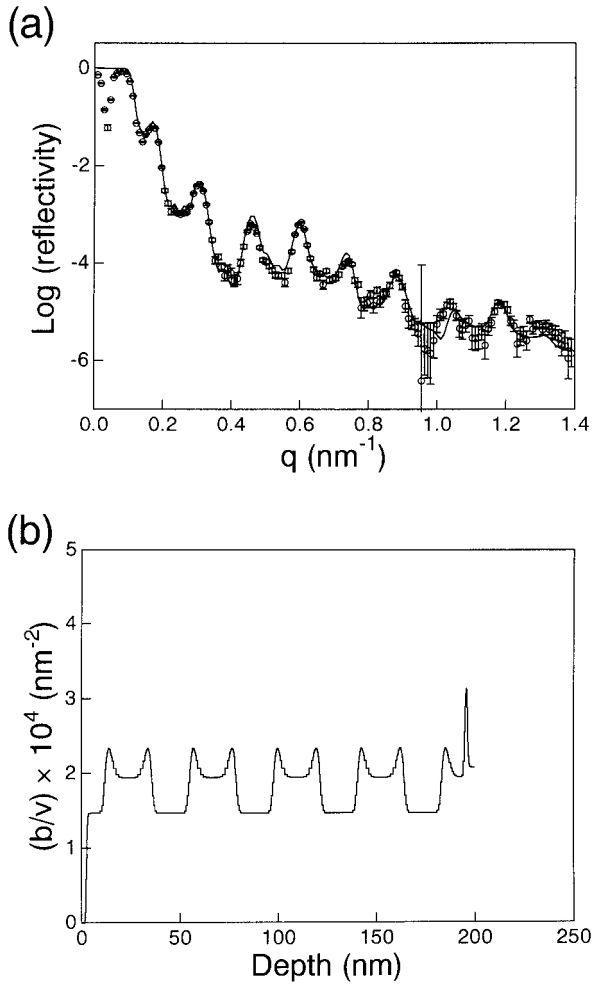

Figure 3. (a) Reflectivity profile of SDP-6 with the D content of 5 vol %. (b) Its scattering length density profile.

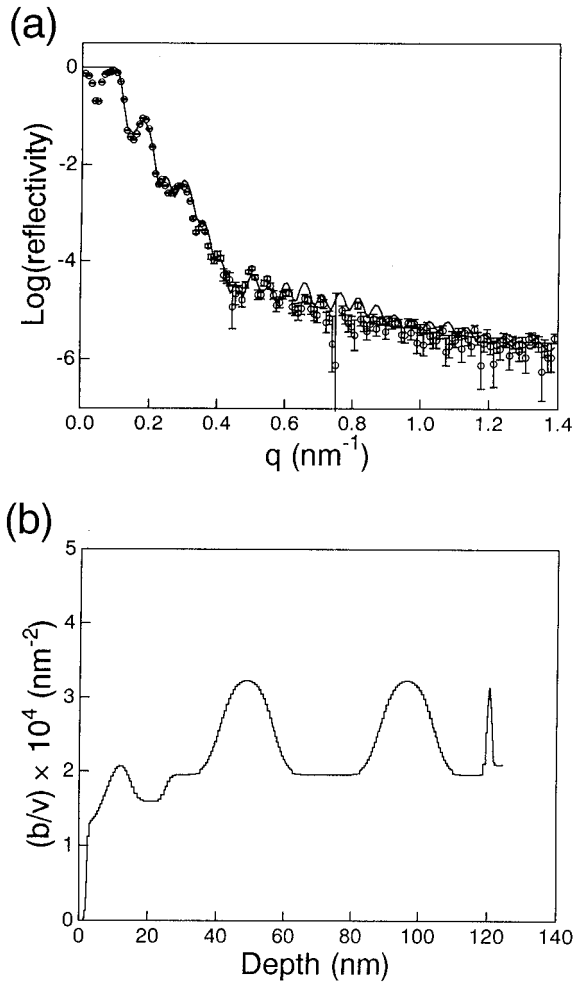

Figure 4. (a) Reflectivity profile of an end-labeled block copolymer, DSP-2, with the D content of 32 vol %. (b) Its scattering length density profile.

found to be the same as that of DP-77, which is about 4.5 nm. In both samples the sharp peaks on the right sides of their *b*/*v* profiles correspond to the SiO_2 layer on the silicon surfaces similarly to DP-77. Moreover, the film surface must be quite uneven because the *b*/*v* value of the topmost polystyrene lamella was much lower than those of the corresponding lamellae inside of the film, as shown in Figure 2b. This aspect of surface roughness will be discussed later. Although the peak *b*/*v* value for SDP-5 (4.0×10^{-4} nm^{-2}) is higher than that for SDP-6 (2.3×10^{-4} nm^{-2}), the former is still lower than the value of the pure D segment, 6.47×10^{-4} nm^{-2}.

Figures 4 and 5 show the reflectivities and the best-fitted *b*/*v* profiles of end-labeled block copolymers with differing D contents, DSP-2 and -3, respectively. Bragg peaks in both reflectivity profiles are weaker than those for DP-77, SDP-5, and SDP-6 shown in Figures 1−3, indicating that the D segments are distributed much more diffusely, at least along the direction perpendicular to the film surface. The best-fitted broad peaks in these *b*/*v* profiles, also, are produced by changing the combination of error functions as described above. This may not be an optimal choice of functions, however, and may be the reason why the agreement between the calculated and the experimental reflectivities is not as good for end-labeled block copolymers. The *b*/*v* profiles of both the end-labeled block copolymers have broad peaks at the centers of the polystyrene lamellae, and their peak *b*/*v* values increase with increasing D content of the block copolymers. The domain spacings, L_{NR}'s, of DSP-2 and -3 were evaluated to be 47 and 43 nm, respectively, from Figures 4b and 5b. Further, both the top film surfaces must be considerably imperfect, since the *b*/*v* values at the film surfaces were much lower than those in the internal sections of the films. The peak *b*/*v* value for DSP-2 was lower than the twin peaks for SDP-5, even though both had almost the same D content. Pure poly(styrene-h_8) phases with $b/v = 1.41 \times 10^{-4}$ nm^{-2} were not observed at either side of the broad peaks in polystyrene microdomains even for DSP-3 in spite of its low D content. These facts imply that the segments on the chain ends are widely distributed over the entire polystyrene lamellar microdomains.

These end-labeled block copolymers are composed of three components, styrene-d_8 (D), styrene-h_8 (S), and 2-vinylpyridine (2VP) segments, and the lamellar structures formed are oriented along the direction parallel to the film surfaces. To determine the volume fraction distribution of labeled and unlabeled segments, we do the following. Assuming incompressibility, we have the following relations for the *b*/*v* profiles shown in Figures 4b and 5b

$$(b/v)(z) = \sum_i (b/v)_i \phi_i(z) \quad (1)$$

$$\sum_i \phi_i(z) = 1 \quad (2)$$

where $(b/v)_i$ and $\phi_i(z)$ are the *b*/*v* value of pure i segment

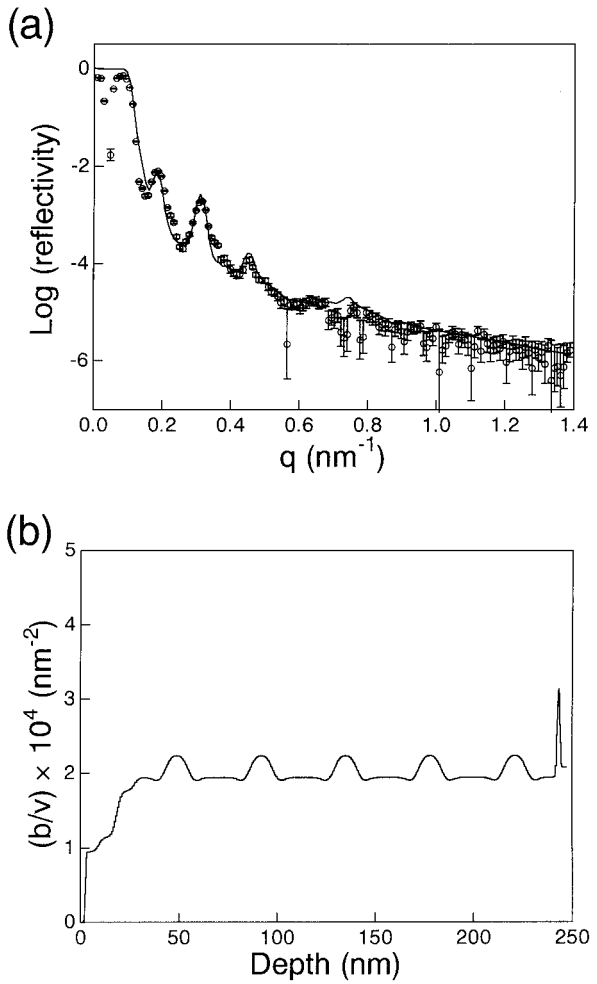

Figure 5. (a) Reflectivity profile of DSP-3 with the D content of 13 vol %. (b) Its scattering length density profile.

(i = D, S, and 2VP) and its volume fraction at z along the direction perpendicular to the film surface, respectively. The $\phi_i(z)$'s in the lamellar microdomain were derived from the above equations assuming that $\phi_{2VP} = 0$ in polystyrene lamellae, while $\phi_D + \phi_S = 0$ in P2VP lamellae. At the lamellar interfaces both the segment distributions of styrene (D + S) and 2VP were assumed to be described by error functions with full-width half-maximum values of 4.5 nm. The results for DSP-2 and -3 are shown in Figures 6 and 7, respectively. The distributions of D segments, indicated by the thick solid lines in the figures, exhibit a broad peak at the center of each polystyrene lamella.

Discussion

The thicknesses of the polystyrene lamella, $L_{PS,NR}$, and poly(2-vinylpyridine) lamella, $L_{P2VP,NR}$, and their total values, L_{NR} (=$L_{PS,NR}$ + $L_{P2VP,NR}$), evaluated from NR measurements, and the resulting polystyrene volume fractions, $\Phi_{PS,NR}$, are listed in Table 3. The L_{NR}'s for the thin films are in good agreement with the lamellar domain spacings, L_{SAXS}'s, evaluated from SAXS measurement for the thick film specimens within experimental errors, suggesting that these lamellar structures are in equilibrium owing to annealing treatment. Further, the $\Phi_{PS,NR}$'s agree well with the analytical polystyrene volume fractions for all the block copolymers used. These facts justify the models used for calculation of reflectivities, in which a high degree of orientation of the lamellar structure along the direction parallel to the silicon surface was assumed.

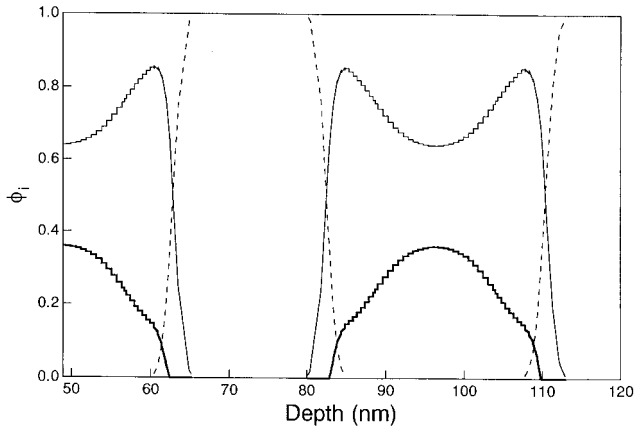

Figure 6. Volume fraction profiles of styrene-d_8 (D), styrene-h_8 (S), and 2-vinylpyridine (2VP) segments of an end-labeled DSP-2, derived from the scattering length density profile shown in Figure 4b. The thick solid line, the thin solid line, and the broken line denote the volume fraction $\phi_D(z)$ of the D segment, $\phi_S(z)$ of the S segment, and $\phi_{2VP}(z)$ of the 2VP segment, respectively.

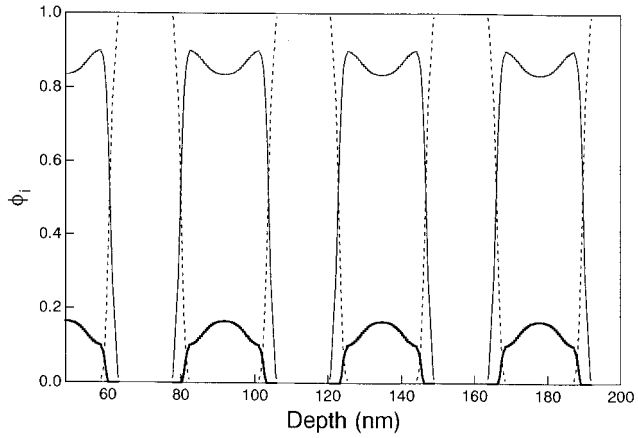

Figure 7. Volume fraction profiles of D, S, and 2VP segments of an end-labeled DSP-3, derived from the scattering length density profile shown in Figure 5b. The different lines denote the volume fractions of different segments in the same manner as in Figure 6.

Table 3. Comparison between the Microdomain Thicknesses in Thin Films and in Bulk

sample code	$L_{PS,NR}$[a] (nm)	$L_{P2VP,NR}$[a] (nm)	L_{NR}[a] (nm)	L_{SAXS} (nm)	$\Phi_{PS,NR}$[b]	Φ_{PS}
DP-77	34.4	34.3	68.7	76.9	0.50	0.50
SDP-5	21.8	21.6	43.4	47.3	0.50	0.51
SDP-6	26.2	16.6	42.8	47.9	0.61	0.58
DSP-2	27.4	20.0	47.4	48.4	0.58	0.57
DSP-3	23.4	19.6	43.0	45.8	0.54	0.54

[a] $L_{PS,NR}$, $L_{P2VP,NR}$, and L_{NR} are the thicknesses of polystyrene and poly(2-vinylpyridine) lamellae and their sum, respectively, evaluated by NR measurements. [b] $\Phi_{PS,NR} = L_{PS,NR}/L_{NR}$.

It has been found previously by optical microscopy[24,25] and atomic force microscopy[26] that there are "holes" or "islands", whose depths or heights are comparable to the lamellar domain spacing, on the film surfaces of block copolymers exhibiting lamellar structures. These "holes" or "islands" can be generated when the film thickness, t, does not satisfy the condition $t = (n + 1/2)L$, where n is an integer and L is the lamellar domain spacing. However, the surface roughnesses of the thin films observed in this study may be different from such "holes" or "islands", since the reflectivity profiles calculated by assuming defects with their depths or heights comparable to lamellar domain spacing located at the

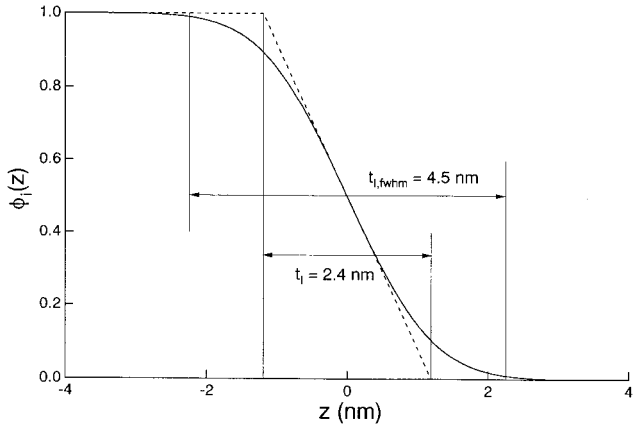

Figure 8. Comparison between the interfacial thickness obtained by two different definitions for sample DP-77. t_I is defined by eq 3 in the text, while $t_{I,fwhm}$ is defined as the full-width half-maximum (fwhm) value of $\phi_i(z)$, where $\phi_i(z)$ is an error function with its fwhm value of 4.5 nm.

top of the films do not fit the experimental reflectivity data. At present, there is no direct evidence for concluding that these PS−P2VPs do not form the "holes" or the "islands" on their film surfaces. It is necessary to observe directly the film surfaces by other techniques for examining the surface roughnesses in more detail.

In the theory of Helfand−Wasserman[10] on microphase separation in the strong segregation limit, the concentration profile at the lamellar interface is assumed to be equal to that in the interface between immiscible homopolymers having infinite molecular weights. In their theory the following definition is used for interfacial thickness

$$t_I = 1/(\mathrm{d}\phi_i(z)/\mathrm{d}z)_{\phi_i=0.5} \tag{3}$$

where $\phi_i(z)$ is the variation of the volume fraction of the i component in the interface along z direction, i.e., the direction perpendicular to the interface, and is predicted to be a hyperbolic tangent function in their mean field approach.[27] Thus the thickness of the lamellar interface, $t_{I,H-W}$, is given by

$$t_{I,H-W} = 2a/(6\chi)^{1/2} \tag{4}$$

where a is the Kuhn statistical segment length and χ is the Flory−Huggins interaction parameter. In this study, on the other hand, the thickness of the interface is defined as the full-width half-maximum (fwhm) value of $\phi_i(z)$. The difference in the definition of interfacial thickness is illustrated in Figure 8. The t_I value of PS−P2VP, for which $\phi_i(z)$ is given by an error function with its fwhm value of 4.5 nm, is calculated to be 2.4 nm by using eq 3. According to eq 4, the $t_{I,H-W}$ of PS−P2VP is estimated to be 2.1 nm by using 0.68 nm[28,29] and 0.073[17] (at T = 423 K) for the segment length and the χ value, respectively. The $t_{I,exp}$ and $t_{I,H-W}$ values thus evaluated for PS−P2VP are listed in Table 4, together with those of PS−PMMA reported by Anastasiadis et al.[15] The $t_{I,exp}$ value of PS−PMMA is higher than that of PS−P2VP, as expected qualitatively from the difference between their χ values. However, these $t_{I,exp}$ values evaluated by NR measurements are apparently higher than the theoretical values, $t_{I,H-W}$. Shull et al.[30,31] and Semenov[32] interpreted quantitatively the difference between the $t_{I,exp}$ and $t_{I,H-W}$ values of PS−PMMA by taking account of two factors: connectivity of immiscible block chains and interfacial fluctuation, which are

Table 4. Comparison between the Experimental and Theoretical Thicknesses of the Lamellar Interface for Styrene−2-Vinylpyridine (PS−P2VP) and Styrene−Methyl Methacrylate (PS−PMMA) Diblock Copolymers

	χ^a	N^b	$t_{I,exp}{}^c$ (nm)	$t_{I,H-W}{}^d$ (nm)	$t_{I,con}{}^e$ (nm)	$t_{I,con+flu}{}^f$ (nm)
PS−P2VP	0.073 (T = 423K)	1530	2.4	2.1	2.5	3.8
PS−PMMA	0.037 (T = 443K)	2830	5.0	3.0	3.6	4.8

[a] χ is the Flory−Huggins interaction parameter. These χ values for PS−P2VP and PS−PMMA were evaluated by using their temperature dependence shown in refs 17 and 16, respectively. [b] N is the degree of polymerization of the block copolymer. [c] $t_{I,exp}$ is the experimental thickness of the lamellar interface evaluated by using the definition of eq 3. [d] $t_{I,H-W}$ is the interfacial thickness given by eq 4. [e] $t_{I,con}$ is the interfacial thickness corrected for connectivity of the block copolymer. [f] $t_{I,con+flu}$ is the thickness corrected for both the connectivity and interfacial fluctuation.

ignored in the theory of Helfand−Wasserman described above. Here, the contributions from the two factors to interfacial thickness were evaluated by the approach of Shull et al., since both the approaches are almost the same. The thickness of the lamellar interface, $t_{I,con}$, corrected for the connectivity was simply evaluated by using Figure 4 in ref 30, where the ratios $t_{I,con}/t_{I,H-W}$ predicted by the mean field theory are plotted as a function of the product of the χ parameter and the degree of polymerization, N, of the block copolymer, though the $t_{I,con}$ value can be evaluated by the mean field theory described in Appendix, which is similar to the theory of Shull. The $t_{I,con}$ values are found to be slightly higher than the $t_{I,H-W}$ values, as shown in Table 4. On the other hand, the contribution from interfacial fluctuation was evaluated by applying the concept of a capillary wave at the fluid interface. The magnitude of interfacial fluctuation is given by[31]

$$(\Delta t_{I,flu})^2 = (k_B T/2\pi\gamma)\ln(\lambda_{max}/\lambda_{min}) \tag{5}$$

where k_B is the Boltzmann constant, T is the absolute temperature, γ is the interfacial tension between polymers, and λ_{max} and λ_{min} are the upper and lower limits of the wavelengths of the fluctuations, respectively. The interfacial tension γ is evaluated from the following relation[27]

$$\gamma = k_B T a \rho_0 (\chi/6)^{1/2} \tag{6}$$

where ρ_0 is the monomer number density. In evaluating the magnitude of fluctuation for the lamellar interface, the lamellar domain spacing, L, and the thickness of the lamellar interface, $t_{I,H-W}$, given by eq 4 were substituted for λ_{max} and λ_{min} in eq 5, respectively. The thicknesses of lamellar interfaces, $t_{I,con+flu}$, corrected for the two factors are shown in Table 4. In the case of PS−P2VP the $t_{I,con}$ value agrees well with the experimental $t_{I,exp}$ value, but the $t_{I,con+flu}$ value is overestimated, in contrast to the case of PS−PMMA. The reason is not apparent, but there is the possibility that the interfacial fluctuations are more suppressed for P2VP on SiO_2 than PMMA, because P2VP can be assumed to have a stronger affinity for SiO_2 than for PMMA. Actually, the adsorption of pyridine[33] onto silica, examined by infrared spectroscopy, is much stronger than that of methyl esters,[34] though these results are not for polymers but for small molecules. Moreover, there is another possibility that the values

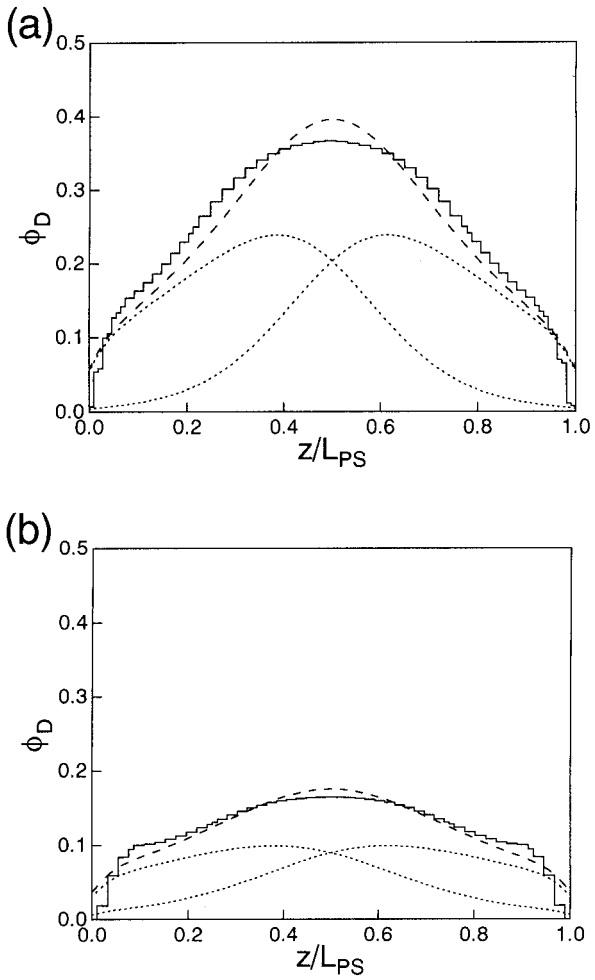

Figure 9. (a) Experimental and theoretical volume fraction, ϕ_D, profiles of the D segment in a lamellar microdomain for DSP-2, where z/L_{PS} is the depth normalized by the thickness, L_{PS}, of a polystyrene lamella. The solid line denotes the experimental ϕ_D profile. The two dotted lines stand for the theoretical ϕ_D profiles of the block chains emitted from the opposite lamellar interfaces and the broken line stands for their sum. (b) Experimental and theoretical volume fraction profiles of the D segment for DSP-3.

of the χ parameter used here may be somewhat unreliable for quantitative discussion on interfacial thickness, because the applicability of Leibler's theory[35] to the SANS data of disordered block copolymers is not confirmed quantitatively.

The segments of block chains adjacent to the chemical junction point connecting two block chains are strongly localized near the lamellar interfaces, as shown in Figures 2b and 3b. These facts are quite reasonable because those junction points themselves are confined to a quite narrow region, i.e., a lamellar interface. The localization of the segments near the chemical junction point is qualitatively consistent with that reported for PS−PMMA by Mayes et al.[14] However, its degree of localization is much higher than that for PS−PMMA, since the thickness of the lamellar interface for PS−P2VP is much thinner than that for PS−PMMA, as discussed above. On the other hand, the segments at the free end are widely distributed within the lamellar microdomains with their distribution maxima at the centers of the microdomains, as shown in Figures 6 and 7. These end-segment distributions are compared to the predictions by a mean field theory in Figure 9, where the volume fraction, ϕ_D, of the D segment in a lamellar microdomain is plotted against the depth z/L_{PS} normalized by the thickness, L_{PS}, of polystyrene lamella. The numerical method for calculating the end-segment distributions is briefly described in the Appendix. The theoretical predictions for both DSP-2 and -3, which are indicated by the broken lines in Figure 9, agree well with their experimental data indicated by the solid lines, which are produced by changing the combination of error functions. The theoretical end-segment distributions are composed of two distributions of the block chains emitted from the opposite interfaces, which are symmetrical with respect the center of the microdomain, shown by the dotted lines in the figure. Thus, the end segments of the block chains from the opposite interfaces are found to be fairly interpenetrated at the center of the lamellar microdomain. Unlike the junction-segment distribution, no large difference between the end-segment distributions is observed for PS−P2VP versus PS−PMMA.[14] This result may not be surprising, since end-segment distributions are controlled by entropic requirements rather than interactions between immiscible block chains.

Acknowledgment. We acknowledge partial support of this work by the Daiko Foundation, and Research Fellowships of the Japan Society for the Promotion of Science for Young Scientists. We are greatly indebted to Dr. John Ankner, University of Missouri, for use of his "mlayer" program to calculate reflectivities. We would like to thank Prof. S. Tsuge, Prof. H. Ohtani, and Y. Ito of Nagoya University for their advice and cooperation in pyrolysis−gas chromatography of partially-deuterated block copolymers, and Prof. M. Kawaguchi of Mie University and Prof. T. Ohta of Ochanomizu University for useful discussions on adsorption of polymers onto silica and the fluctuation of interfaces.

Appendix

In this Appendix, we briefly present the numerical method for the theoretical prediction of the end-segment distribution of a block chain in a lamellar microdomain. According to the mean field theory of Helfand,[9] the statistical weight $Q_K(\tau,z;\tau',z')$, which is the joint probability of finding the τth and the τ'th segments of the K-block chain (K = PS or P2VP in the present case) at positions z and z', respectively, is given by

$$\frac{\partial}{\partial\tau}Q_K(\tau,z;\tau',z') = \left[\frac{a^2}{6}\frac{\partial^2}{\partial z^2} - \beta V_K(z)\right]Q_K(\tau,z;\tau',z') \quad \text{(A.1)}$$

where $\beta = 1/k_BT$ and $V_K(z)$ is the mean field acting on a K segment at position z, given by

$$\beta V_K(z) = \sum_{K'}\epsilon_{KK'}\frac{\phi_{K'}(z)}{\phi_0} + \frac{1}{\kappa}\left[\sum_{K'}\phi_{K'}(z) - \phi_0\right] \quad \text{(A.2)}$$

where $\phi_K(z)$ is the local segment density of the K segment, $\epsilon_{KK'}$ is the interaction energy between the K- and the K′-type segments divided by k_BT, ϕ_0 is the equilibrium value of the total segment density, and κ is the compressibility divided by k_BT. This equation should be supplemented by the following initial condition

$$Q_K(0,z;0,z') = \delta(z-z') \quad \text{(A.3)}$$

$\phi_K(z)$ is calculated by using the $Q_K(\tau,z;\tau',z')$'s as

$$\phi_K(z) = [\int_0^J d\tau \int_L dz_0 \int_L dz_J \int_L dz_N\, Q_K(0,z_0;\tau,z)\, Q_K(\tau,z;J,z_J)\, Q_{K'}(J,z_J;N,z_N)]/[\int_L dz_0 \int_L dz_J \int_L dz_N\, Q_K(0,z_0;J,z_J)\, Q_{K'}(J,z_J;N,z_N)] \quad \text{(A.4)}$$

where $\tau = J$ corresponds to the junction point between the block chains, N is the total degree of polymerization of a block copolymer, and $\int_L dz$ means the integral over the interval L given by $-L_{PS}/2 \le z \le L_{P2VP}/2$ when the origin of the z-axis is at the center of a lamellar interface. Equations A.1−A.4 form a set of self-consistent equations, which should be solved numerically by an iteration method. The diffusion equation (A.1) was solved using the standard Crank−Nicholson implicit finite difference scheme with a spatial mesh width that is sufficiently smaller than the interfacial thickness. Once the $Q_K(\tau,z;\tau',z')$'s are obtained, the density distribution of deuterated segments, $\phi_D(z)$, is calculated using an equation similar to eq A.4 in which the integral $\int_0^J d\tau$ is replaced by $\int_0^{N_D} d\tau$ where N_D is the number of deuterated segments in a chain.

As a check of the above calculation procedure, we confirmed that the calculated lamellar spacings using the $Q_K(\tau,z;\tau',z')$'s with the experimental values of the χ parameter and the numbers of segments in a chain well reproduce the experimentally-obtained lamellar spacings for both DSP-2 and DSP-3 cases.

References and Notes

(1) Molau, G. E. In *Block Copolymers*; Aggarwal, S. L., Ed.; Plenum Press: New York, 1970.
(2) Hasegawa, H.; Tanaka, H.; Yamasaki, K.; Hashimoto, T. *Macromolecules* **1987**, *20*, 1651.
(3) Shibayama, M.; Hashimoto, T.; Kawai, H. *Macromolecules* **1983**, *16*, 1434.
(4) Matsushita, Y.; Mori, K.; Saguchi, R.; Nakao, Y.; Noda, I.; Nagasawa, M. *Macromolecules* **1990**, *23*, 4313.
(5) Hashimoto, T.; Shibayama, M.; Kawai, H. *Macromolecules* **1980**, *13*, 1237.
(6) Matsushita, Y.; Mori, K.; Mogi, Y.; Saguchi, R.; Noda, I.; Nagasawa, M.; Chang, T.; Glinka, C. J.; Han, C. C. *Macromolecules* **1990**, *23*, 4317.
(7) Hasegawa, H.; Hashimoto, T.; Kawai, H.; Lodge, T. P.; Amis, E. J.; Glinka, C. J.; Han, C. C. *Macromolecules* **1985**, *18*, 67.
(8) Meier, D. J. In *Block and Graft Copolymers*; Burke, J. J., Weiss, V., Eds.; Syracuse University Press: Syracuse, NY, 1973.
(9) Helfand, E. *Macromolecules* **1975**, *8*, 552.
(10) Helfand, E.; Wasserman, Z. R. *Macromolecules* **1976**, *9*, 879.
(11) Semenov, A. N. *Sov. Phys. JETP* **1985**, *61*, 733.
(12) Ohta, T.; Kawasaki K. *Macromolecules* **1986**, *19*, 2621.
(13) Matsushita, Y.; Mori, K.; Saguchi, R.; Noda, I.; Nagasawa, M.; Chang, T.; Glinka, C. J.; Han, C. C. *Macromolecules* **1990**, *23*, 4387.
(14) Mayes, A. M.; Johnson, R. D.; Russell, T. P.; Smith, S. D.; Satija, S. K.; Majkrzak, C. F. *Macromolecules* **1993**, *26*, 1047.
(15) Anastasiadis, S. H.; Russell, T. P.; Satija, S. K.; Majkrzak, C. F. *J. Chem. Phys.* **1990**, *92*, 5677.
(16) Russell, T. P.; Hjelm, R. P.; Seeger, P. A. *Macromolecules* **1990**, *23*, 890.
(17) Takahashi, Y.; et al. Manuscript in preparation.
(18) Matsushita, Y.; Nakao, Y.; Saguchi, R.; Choshi, H.; Nagasawa, M. *Polym. J.* **1986**, *18*, 493.
(19) Ohtani, H.; Tsuge, S.; Matsushita, Y.; Nagasawa, M. *Polym. J.* **1984**, *16*, 727.
(20) The reference to commercial equipment does not imply its recommendation or endorsement by the National Institute of Standards and Technology.
(21) Parratt, L. G. *Phys. Rev.* **1954**, *95*, 359.
(22) Russell, T. P. *Mater. Sci. Rep.* **1990**, *5*, 171.
(23) The χ^2 values indicating the quality of the fit of the calculated reflectivity profile to the experimental one are between 20 and 330 for all the samples studied in this work.
(24) Coulon, G.; Ausserre, D.; Russell, T. P. *J. Phys. Fr.* **1990**, *51*, 777.
(25) Coulon, G.; Collin, B.; Ausserre, D.; Chatenay, D.; Russell, T. P. *J. Phys. Fr.* **1990**, *51*, 2801.
(26) Collin, B.; Chatenay, D.; Coulon, G.; Ausserre, D.; Gallot, Y. *Macromolecules* **1992**, *25*, 1621.
(27) Helfand, E.; Tagami, Y. *J. Chem. Phys.* **1972**, *56*, 3592.
(28) Ballard, D. G. H.; Wignall, G. D.; Schelten, J. *Eur. Polym. J.* **1973**, *9*, 965.
(29) Matsushita, Y.; Shimizu, K.; Nakao, Y.; Choshi, H.; Noda, I.; Nagasawa, M. *Polym. J.* **1986**, *18*, 361.
(30) Shull, K. R. *Macromolecules* **1992**, *25*, 2122.
(31) Shull, K. R.; Mayes, A. M.; Russell, T. P. *Macromolecules* **1993**, *26*, 3929.
(32) Semenov, A. N. *Macromolecules* **1993**, *26*, 6617.
(33) Griffiths, D. M.; Marshall, K.; Rochester, C. H. *J. Chem. Soc., Faraday Trans. 1* **1974**, *70*, 400.
(34) Mills, A. K.; Hockey, J. A. *J. Chem. Soc., Faraday Trans. 1* **1975**, *71*, 2398.
(35) Leibler, L. *Macromolecules* **1980**, *13*, 1602.

MA961089P